ISSN 2047-3338

Multimodal Image Fusion Technique MIFT-DWNRT for Improvement of Medical Diagnosis Abilities

Manvi[1] and Ashish Oberoi[2]
[1,2]RIMT University, Mandi-Gobindgarh – 147301, Punjab, India
[1]manvi7@gmail.com, [2]a_oberoi01@yahoo.co.in

***Abstract*– In this article, a novel multimodal Medical Image Fusion Technique (MIFT) in light of MIFT-HDWRT, Non-sub sampled Contourlet Transform (NSCT) and Pulse-Coupled Neural Network (PCNN) is displayed. The MIFT-DWNRT plot tells the advantages of both the NSCT and PCNN to acquire better combination results. The source medical images are first decayed by NSCT. The low-recurrence sub bands (LFSs) are intertwined utilizing the MIFT-HDWRT run the show. For melding the high-recurrence sub bands (HFSs) a NSCT-PCNN show is used. Altered Spatial Frequency (MSF) in NSCT space is contribution to propel the PCNN, and coefficients in NSCT area with expansive terminating times are chosen as coefficients of the intertwined image. At long last, opposite of NSCT i.e., INSCT is connected to get the intertwined image. Abstract and target examination of the outcomes and correlations with cutting edge MIF technique demonstrate the effectiveness of the MIFT-DWNRT plot in melding multimodal therapeutic images.**

***Index Terms*– Image Fusion, Pulse-Coupled Neural Network, Multiscale Geometric Analysis, Medical Imaging and NSCT**

I. INTRODUCTION

IN the course of the most recent couple of decades, therapeutic imaging is playing an inexorably basic and crucial part in countless applications including determination, re-pursuit, treatment, and training. To offer help to the doctors various modalities of restorative images have turned out to be accessible, reflecting different information of human organs, tissues, and having their separate application ranges. For example, auxiliary restorative images like Magnetic Resonance Imaging (MRI), Computed Tomography (CT), Ultrasonography (USG), and Magnetic Resonance Angiography (MRA) furnish high goals images with anatomical data. Though, utilitarian medicinal images, for example, Position Emission Tomography (PET), Single-Photon Emission CT (SPECT), and functional MRI (fMRI) furnish low-spatial goals images with useful data. A solitary methodology of medicinal image can't give far reaching and exact information. In this manner, joining multimodal therapeutic images to give considerably more valuable data through image fusion has turned into the focal point of imaging research [1].

Up until this point, numerous Image Fusion (IF) strategies are taken into account by different specialists. It has been discovered that the pixel-level spatial space image fusion techniques more often than not prompt difference decrease. Strategies in view of Intensity-Hue-Saturation (IHS), Principal Component Analysis (PCA), and Brovey Transform offer better outcomes, however, suffer from otherworldly corruption [2]. Pyramidal image fusion plans to such an extent that laplacian pyramid, slope pyramid, differentiate pyramid, proportion of low-pass pyramid, and morpho-sensible pyramid neglect to present any spatial introduction selectivity in the deterioration procedure, and subsequently frequently cause blocking effects [3]. The broadly utilized Discrete Wavelet Transform (DWT) can protect ghastly data efficiently yet can't express spatial qualities effectively [5]. Subsequently, DWT based combination plans can't save the notable highlight of the source images efficiently, and present antiques, and irregularities in the melded results [6]. As of late, a few Multiscale Geometric Analysis (MGA) devices are produced, for example, Curvelet, Contourlet, Non-sub Sampled Contourlet Transform (NSCT), and Ripplet which don't suffer from the problems of wavelet. Numerous image fusion and MIF techniques in view of these Multiscale Geometric Analysis (MGA) instruments are developed [7].

Pulse Coupled Neural Network (PCNN) is a visual cortex-motivated neural system portrayed by the worldwide coupling and heartbeat synchronization of neurons [8]. It has been seen that PCNN based image fusion plans outflank the traditional image fusion strategies [10]. Despite the fact that there exist a few image fusion plans in light of change area and PCNN, a large portion of these strategies suffer from different issues. A technique quick MIF conspire in view of a multi-channel PCNN (m-PCNN) show with simple extensibility capacity, delivering combined images with high data content, yet suffering from the issues of differentiation decrease and loss of image fine points of interest [11]. A new technique comes up in consideration of image fusion strategy in view of spatial recurrence (SF) propelled PCNN in NSCT space [12]. It functions admirably for multi-focus image fusion, and unmistakable image fusion, however the nonappearance of directional data in spatial recurrence, and the utilization of same combination manage for both the sub-bands cause

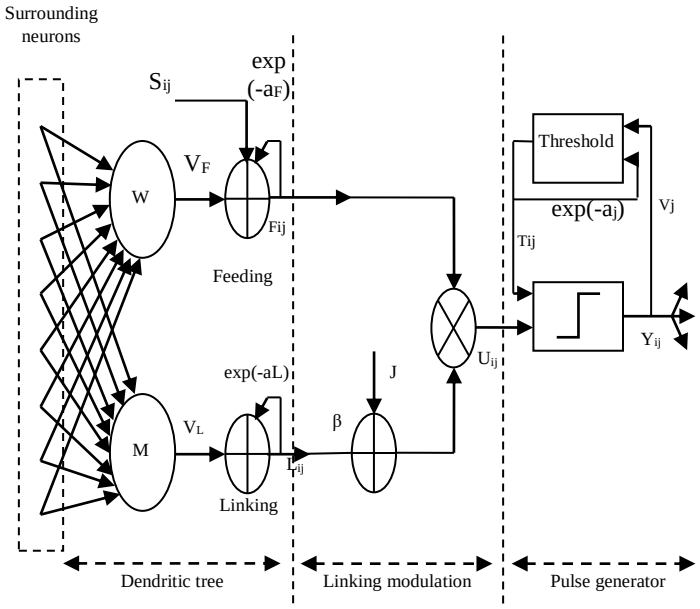

Fig. 1: Structure of PCNN

differentiate decrease, and loss of image subtle elements as shown in Fig. 1. The image fusion strategy of double layer PCNN demonstrate with a negative criticism control system in the NSCT area has indicated promising outcomes in multi-focus image fusion [13]. A technique for MIF and edge reasoning in light of NSCT and PCNN is developed. This plan additionally suffers from the issues of complexity decrease and undesirable image debasements. The strategy of bi-dimensional experimental mode disintegration and m-PCNN, indicates great bring about protecting the source images fine points of interest in the melded image, however, suffers from differentiate decrease [14]. In a large portion of the current image fusion strategies in light of PCNN the estimation of a solitary pixel (coefficient) in spatial or change space is utilized to inspire one neuron [15]. Be that as it may, this straightforward utilization of pixels (coefficients) in spatial or change area isn't sufficiently effective, in light of the fact that people are touch to edges, and directional highlights. Additionally, it has likewise been discovered that utilizing different combination rules for different sub-bands result in better melded images.

The field of MIF is very different from that of multi-focus and noticeable image fusion. A large portion of the occasions, there are extremely unobtrusive differences between the highlights of the source medicinal images.

Exceptional care must be taken amid the combination procedure of these fine subtle elements. In this manner, MIF plot is required that can at the same time handle the issues of differentiation decrease, loss of image subtle elements, and undesirable image debasements. The fundamental commitment of MIFT-DWNRT technique is to utilize the move invariance, multi-scale, and multi-directional properties of NSCT alongside the altered spatial recurrence (fit for catching the fine points of interest show in the Fig. 2 persuaded PCNN so that can catch the unobtrusive differences and the fine subtle elements display in the source medicinal images that outcome in intertwined images with high complexity, lucidity, and data content.

II. NON-SUBSAMPLED CONTOURLET TRANSFORM

Non-subsampled Contourlet Transform (NSCT) is a completely move invariant, multi-scale and multi-direction expansion that has a quick usage. The Contourlet Transform (CT) isn't move invariant because of the nearness of the down-samplers, and up-samplers in both the Laplacian Pyramid, and Directional Filter Bank (DFB) phases of Controulet Transform [16]. NSCT accomplishes move invariance property by utilizing the Non-subsampled pyramid channel bank (NSP or NSPFB) and the Non-subsampled DFB (NSDFB).

III. NON-SUBSAMPLED PYRAMID FILTER BANK

Non-subsampled Pyramid Filter Bank (NSPFB) is a move invariant sifting structure representing the multi-scale property of the NSCT. This is accomplished by utilizing two-channel Non-subsampled banks. It has no down-sampling or up-sampling and, thus moves invariant. Idealize reproduction is accomplished given the channels fulfill the accompanying character.

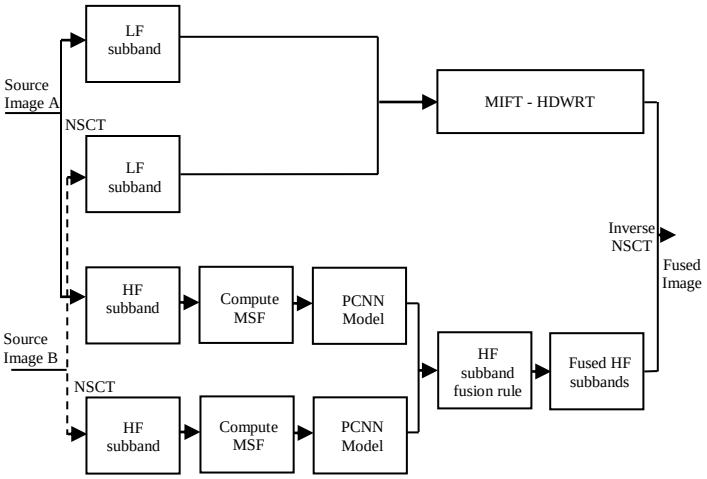

Fig. 2: Block diagram of MIFT – DWNRT Technique

$$H_0(z)\,G_0(z) + H_1(z)\,G_1(z) = 1 \qquad (1)$$

Where, $H_0(z)$ is the low-pass decomposition filter, $H_1(z)$ is the high-pass decomposition filter, $G_0(z)$ is the low-pass reconstruction filter, and $G_1(z)$ is the high-pass reconstruction filter.

With a specific end goal to acquire the multi-scale disintegration, Non-subsampled Pyramid Filter Bank is built by iterated Non-subsampled channel banks. For the following level all channels are up-sampled by two in the two measurements. Hence, they likewise fulfill the ideal recreation character. The proportional channels of a k-th level falling Non-subsampled Pyramid Filter Bank are given by:

$$H_n^{eq}(z) = \begin{cases} H_1(z^{2^{n-1}}) \prod_{j=0}^{n-2} H_0(z^{2^j}), 1 \le n < 2^k \\ \prod_{j=0}^{n-1} H_0(z^{2^j}), \quad n = 2^k \end{cases} \quad (2)$$

where z^j stands for $[z_1^j, z_2^j]$.

IV. NON-SUBSAMPLED DIRECTIONAL FILTER BANK

Non-subsampled Directional Filter Bank (NSDFB) is built by disposing of the down-samplers and up-samplers of the directional filter bank by exchanging off the down-samplers/ up-samplers in every two divert channel bank in the directional filter bank tree structure, and up-sampling the channels appropriately [17]. The yields of the main level, and second level channels are joined to get four directions recurrence decay. The blend channel bank is acquired also. All channel banks in the Non-subsampled Directional Filter Bank (NSDFB) tree structure are acquired from a solitary NSFB with fan channels. To get multidirectional decay the NSDFBs are iterated and to get the following level disintegration all channels are up inspected by a quincunx network given by:

$$QM = \begin{bmatrix} 1 & 1 \\ 1 & -1 \end{bmatrix} \quad (3)$$

The NSCT is gotten by joining the 2-D NSPFB and the NSDFB. The subsequent separating structure approximates the perfect segment of the recurrence plane. It must be noticed that difference from the contourlet development the NSCT has a redundancy given by $R = \sum^j 2^l j$, where $2^l j$ is the number of directions at scale j.

V. PULSE COUPLED NEURAL NETWORK

Pulsed Coupled Neural Network (PCNN) is a solitary layered, two-dimensional; along the side associated neural system of heart beat coupled neurons. The PCNN neurons structure is appeared in Fig. 1. The neuron comprises of an info part (dendritic tree), connecting part and a heartbeat generator. The neuron gets the information signals from nourishing and connecting inputs. Sustaining input is the essential contribution from the neurons responsive zone. The neuron responsive zone comprises of the neighboring pixels of relating pixel in the information image. Connecting input is the optional contribution of horizontal associations with neighboring neurons. The difference between these sources of information is that the nourishing associations have a slower trademark reaction time steady than the connecting associations. The standard PCNN display is portrayed as emphasis by the accompanying conditions [18].

$$F_{i,j}[n] = e^{-\alpha_F} F_{i,j}[n-1] + V_F \sum_{k,l} w_{i,j,k,l} Y_{i,j}[n-1] + S_{i,j} \quad (4)$$

$$L_{i,j}[n] = e^{-\alpha_L} L_{i,j}[n-1] + V_L \sum_{k,l} m_{i,j,k,l} Y_{i,j}[n-1] \quad (5)$$

$$U_{i,j}[n] = F_{i,j}[n]\left(1 + \beta L_{i,j}[n]\right) \quad (6)$$

$$Y_{i,j}[n] = \begin{cases} 1, U_{i,j}[n] > T_{i,j}[n] \\ 0, \quad \text{otherwise} \end{cases} \quad (7)$$

$$T_{i,j}[n] = e^{-\alpha T} T_{i,j}[n-1] + V_T Y_{i,j}[n] \quad (8)$$

In Eq. (4) to Eq. (8), the lists I and j elude to the pixel area in the image, k and l elude to the separation in a symmetric neighborhood around one pixel, and n signifies the present emphasis (discrete time step). Here n shifts from 1 to N (total number of cycles). The dendritic tree is given by Eq. (4) and Eq. (5). The two primary parts F and L are called bolstering and connecting, individually. $w_{i,j,k,l}$ and $m_{i,j,k,l}$ are the synaptic weight coefficients and S is the outside boost. V_F and V_L are normalizing constants. F and L are the time constants, and F < L. The connecting tweak is given in Eq. (6), where $U_{i,j}[n]$ is the inside condition of the neuron and is the connecting parameter. The beat generator decides the terminating occasions in the model in Eq. (7). $Y_{i,j}[n]$ relies upon the inside state and limit. The dynamic edge of the neuron is Eq. (8), where V_T and T is standardized consistent and time steady, individually.

VI. MIFT-DWNRT TECHNIQUE

The documentations utilized in this segment are as per the following: A, B, R speaks to the two source images and the resultant melded image, separately. C = (A; B; R). $L^C{}_G$ shows the low-recurrence sub-band (LFS) of the image C at the coarsest scale G. D, G, h, and C speaks to the high-recurrence sub-band (HFS) of the image C at scale g, (g = 1; ; G) and bearing h. (i, j) signifies the spatial area of each coefficient. The strategy can be effortlessly stretched out to in excess of two images.

A) Fusing Low Frequency Sub-bands

The Low Frequency Sub-bands (LFSs) coefficients are melded utilizing MIFT-HDWRT run the show. As indicated by this combination lead, select the recurrence coefficients from $L^A{}_G$ or $L^B{}_G$ with more noteworthy total an incentive as the intertwined coefficients.

$$L_G^R(i,j) = \begin{cases} L_G^A(i,j), \left|L_G^A(i,j)\right| \ge \left|L_G^B(i,j)\right| \\ L_G^B(i,j), \quad \text{otherwise} \end{cases} \quad (9)$$

B) Fusing High Frequency Sub-bands

The High Frequency Sub-bands (HFSs) of the source images are intertwined utilizing Pulse Coupled Neural Network (PCNN). As people are touchy to highlights, for example, edges, shapes and so forth., so as opposed to utilizing PCNN in Non-Subsampled Contourlet Transform (NSCT) space straightforwardly (i.e., utilizing individual coefficients), changed spatial recurrence (MSF) in NSCT area is considered as the image highlight to rouse the PCNN.

Spatial recurrence (SF) is figured by line and section recurrence. It mirrors the entire action level of an image which implies the bigger the SF the higher the image goals. This technique utilized an adjusted rendition of SF in the MIFT-DWNRT technique. The MSF comprises of line (RF), section (CF) and askew recurrence (DF). The first SF does

not have the directional data exhibit in the image which results in the loss of critical fine points of interest of the image. Though, MSF fuses this directional data and outcomes in a image clearness/action level measure equipped for catching the fine points of interest. For M x N pixel image the MSF is characterized as be the modified spatial.

$$\mathrm{MSF} = \sqrt{\mathrm{RF}^2 + \mathrm{CF}^2 + \mathrm{DF}^2} \tag{10}$$

where,

$$\mathrm{RF} = \sqrt{\frac{1}{\mathrm{M}(\mathrm{N}-1)} \sum_{\mathrm{m}=1}^{\mathrm{M}} \sum_{\mathrm{n}=2}^{\mathrm{N}} \left[\mathrm{f}_{\mathrm{m,n}} - \mathrm{f}_{\mathrm{m,n-1}}\right]^2} \tag{11}$$

$$\mathrm{CF} = \sqrt{\frac{1}{(\mathrm{M}-1)\mathrm{N}} \sum_{\mathrm{m}=2}^{\mathrm{M}} \sum_{\mathrm{n}=1}^{\mathrm{N}} \left[\mathrm{f}_{\mathrm{m,n}} - \mathrm{f}_{\mathrm{m-1,n}}\right]^2} \tag{12}$$

and,

$$\mathrm{DF} = \mathrm{P} + \mathrm{Q} \tag{13}$$

where,

$$\mathrm{P} = \sqrt{\frac{1}{(\mathrm{M}-1)(\mathrm{N}-1)} \sum_{\mathrm{m}=2}^{\mathrm{M}} \sum_{\mathrm{n}=2}^{\mathrm{N}} \left[\mathrm{f}_{\mathrm{m,n}} - \mathrm{f}_{\mathrm{m-1,n-1}}\right]^2} \tag{14}$$

and,

$$\mathrm{Q} = \sqrt{\frac{1}{(\mathrm{M}-1)(\mathrm{N}-1)} \sum_{\mathrm{m}=2}^{\mathrm{M}} \sum_{\mathrm{n}=2}^{\mathrm{N}} \left[\mathrm{f}_{\mathrm{m-1,n}} - \mathrm{f}_{\mathrm{m,n-1}}\right]^2} \tag{15}$$

where, the feeding input $\mathrm{F}_{\mathrm{i,j}}^{\mathrm{g,h,C}}$ is equal to the modified spatial frequency $MSF_{\mathrm{i,j}}^{\mathrm{g,h,C}}$. The linking input $\mathrm{L}_{\mathrm{i,j}}^{\mathrm{g,h,C}}$ is equal to the sum of neurons firing times in linking range $\mathrm{W}_{\mathrm{i,j,k,l}}$ is the synaptic gain strength and subscripts *k* and *l* are the size of measured by using an overlapping window around the concerned coefficient where *C* = (*A*, *B*). In order to reduce the computational complexity, the simplified PCNN is used.

$$\mathrm{F}_{\mathrm{i,j}}^{\mathrm{g,h,C}}[\mathrm{n}] = \mathrm{MSF}_{\mathrm{i,j}}^{\mathrm{g,h,C}} \tag{16}$$

$$\mathrm{L}_{\mathrm{i,j}}^{\mathrm{g,h,C}}[\mathrm{n}] = \mathrm{e}^{-\propto \mathrm{L}} \mathrm{L}_{\mathrm{i,j}}^{\mathrm{g,h,C}}[\mathrm{n}-1] + \mathrm{V}_{\mathrm{L}} \sum_{\mathrm{k,l}} \mathrm{W}_{\mathrm{i,j,k,l}}^{\mathrm{g,h,C}} \mathrm{Y}_{\mathrm{i,j,k,l}}^{\mathrm{g,h,C}}[\mathrm{n}-1] \tag{17}$$

$$\mathrm{U}_{\mathrm{i,j}}^{\mathrm{g,h,C}}[\mathrm{n}] = \mathrm{F}_{\mathrm{i,j}}^{\mathrm{g,h,C}}[\mathrm{n}] * \left(1 + \beta \mathrm{L}_{\mathrm{i,j}}^{\mathrm{g,h,C}}[\mathrm{n}]\right) \tag{18}$$

$$\theta_{\mathrm{i,j}}^{\mathrm{g,h,C}}[\mathrm{n}] = \mathrm{e}^{-\alpha_\theta} \theta_{\mathrm{i,j}}^{\mathrm{g,h,C}}[\mathrm{n}-1] + \mathrm{V}_\theta \mathrm{Y}_{\mathrm{i,j}}^{\mathrm{g,h,C}}[\mathrm{n}-1] \tag{19}$$

$$\mathrm{Y}_{\mathrm{i,j}}^{\mathrm{g,h,C}}[\mathrm{n}] = \begin{cases} 1, \mathrm{U}_{\mathrm{i,j}}^{\mathrm{g,h,C}}[\mathrm{n}] > \theta_{\mathrm{i,j}}^{\mathrm{g,h,C}}[\mathrm{n}] \\ 0, \quad \text{otherwise} \end{cases} \tag{20}$$

$$\mathrm{T}_{\mathrm{i,j}}^{\mathrm{g,h,C}}[\mathrm{n}] = \mathrm{T}_{\mathrm{i,j}}^{\mathrm{g,h,C}}[\mathrm{n}-1] + \mathrm{Y}_{\mathrm{i,j}}^{\mathrm{g,h,C}}[\mathrm{n}] \tag{21}$$

The linking range in the PCNN is the decay constant L. The linking strength, V_{L} and V are the amplitude gains. $\mathrm{U}_{\mathrm{i,j}}^{\mathrm{g,h,C}}$ is the total internal activity and i,j,g,h, and C is the threshold. If $\mathrm{U}_{\mathrm{i,j}}^{\mathrm{g,h,C}}$ is larger then $\theta_{\mathrm{i,j}}^{\mathrm{g,h,C}}$, then the neuron will generate a pulse $\mathrm{Y}_{\mathrm{i,j}}^{\mathrm{g,h,C}} = 1$ also called one firing time. The sum of $\mathrm{Y}_{\mathrm{i,j}}^{\mathrm{g,h,C}} = 1$ in n iteration (namely the firing times), is used to represent the image information. Here, rather than $\mathrm{Y}_{\mathrm{i,j}}^{\mathrm{g,h,C}}[\mathrm{n}]$, $\mathrm{T}_{\mathrm{i,j}}^{\mathrm{g,h,C}}[\mathrm{n}]$ is analyzed, since neighboring coefficients with similar features represent similar firing times in a given iteration time.

C) Algorithm

The restorative images to be combined must be enlisted to guarantee that the comparing pixels are adjusted. The new algorithm MIFT-DWNRT image fusion is given below:

- *Step I:* Read the set of multimodal images (i.e., two images of different modality of same size).
- *Step II:* Decompose the registered source medical images X and Y by Non-subsampled Contourlet Transform (NSCT).
- *Step III:* Apply discrete wavelet transformation on NSCT image to get the Low Frequency Sub-bands (LFSs), and High Frequency Sub-bands (HFSs).
- *Step IV:* Compute the linking strengths.
- *Step V:* Input the coefficients of the sub bands to motivate the reduced pulse-coupled neural network (RPCNNs) and generate pulse of neurons.
- *Step VI:* At n = N (total number of iterations), determine the fused coefficient and apply the fusion rule.
- *Step VII:* Apply Ripplet transform.
- *Step VIII:* Apply inverse discrete wavelet transformation.
- *Step IX:* Apply inverse NSCT on the DWT coefficients to get the final fused medical image.
- *Step X:* Display the final fused image.

VII. SIMULATION RESULTS

The medical images used for the fusion are CT and MRI. The combination used for fusion is CT with MRI is shown in Fig. 3(a), Fig. 3(b) and Fig. 4(a), Fig. 4(b), respectively:

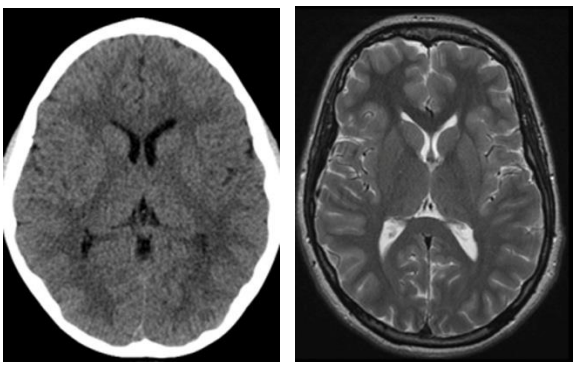

(a) (b)

Fig.3. input images (a) CT image; (b) MRI image

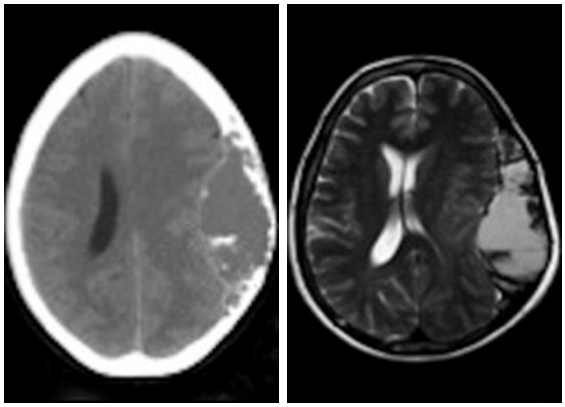

(a) (b)

Fig. 4: Input images (a) CT image; (b) MRI image

Simulation was carried out using MATLAB version 2016. The fused output obtained using MIFT-DWNRT and qualitative analysis is shown in Fig. 5.

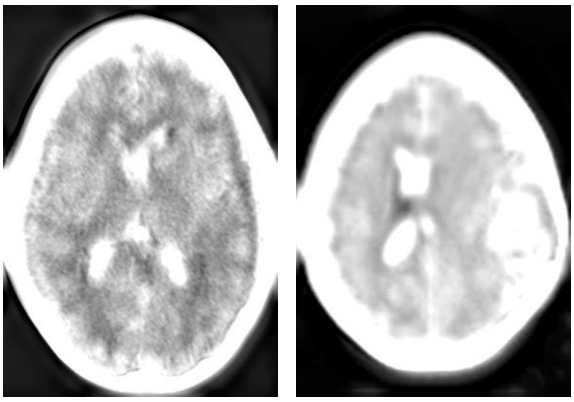

Fig. 5: fused output of CT with MRI using MIFT-DWNRT

Qualitative analysis is used for the subjective evaluation of the images. As subjective evaluation differs based on visual acuity, quantitative analysis is necessary for analyzing the quality of the fused image. Different parameters like PSNR, Entropy, Standard Deviation (SD), and Structural Similarity Index Measure (SSIM) are evaluated on 10 sets of images and compared with the existing methods for proving the effectiveness of the MIFT-DWNRT technique. Table I shows the value of quality measures implemented on MIFT-DWNRT, and existing method.

Table I: Qualitative Analysis of MIFT-DWNRT and Existing Method

Input Image	Quality Factor	MIFT-DWNRT	Existing Method
CT with MRI	PSNR	9.0441	7.7648
	Entropy	6.7323	6.2843
	SD	23.0891	9.2253
	SSIM	0.3560	0.1407
CT with MRI	PSNR	9.5938	5.5009
	Entropy	5.6612	3.3568
	SD	50.2766	20.1974
	SSIM	0.6164	0.277

The quality metrics PSNR, Entropy, SD, and SSIM are shown graphically in Fig. 6, and Fig. 7 for comparison based on Table I, respectively:

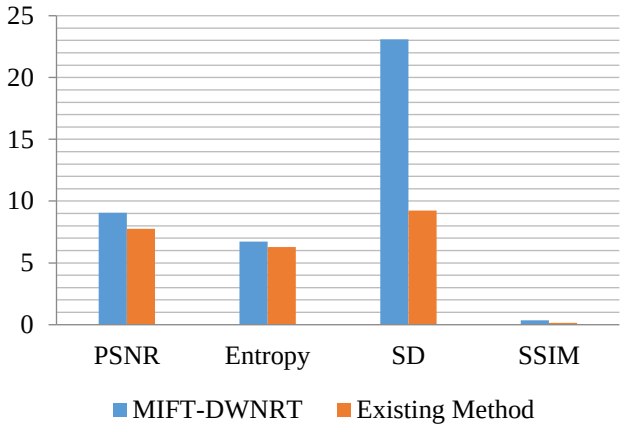

Fig. 6: Qualitative Analysis of CT with MRI fusion

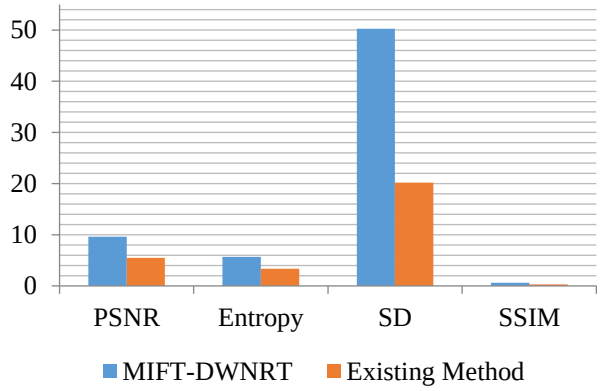

Fig. 7: Qualitative Analysis of CT with MRI fusion

VIII. CONCLUSION

A specialist radiologist was solicited to abstractly assess the effectiveness from the MIFT-DWNRT technique. After watchful manual investigation of the images of the Fig. 3, Fig. 4, and Fig. 5 the radiologist adjusted to the effectiveness of the MIFT-DWNRT. The intertwined images gotten by the MIFT-DWNRT conspire are clearer, in-developmental and have higher difference than the source restorative images that is useful in perception and in addition understanding. The resultant intertwined images gotten by NSCT, and PCNN are outwardly especially like the fused images acquired by the MIFT-DWNRT technique. Yet, amid the quantitative investigation, the fused images acquired by the MIFT-DWNRT conspire have higher quantitative outcomes than the existing technique. The MIFT-DWNRT technique is conspired less undesirable corruptions in the fused images, and in addition is free from the issue of blocking effect. Consequently, it is obvious from the abstract investigation of the fused images that the MIFT-DWNRT technique is exceptionally effective in fusing multi-model restorative images.

Table I demonstrates the PSNR, Entropy, Standard Deviation (SD), and Structural Similarity Index Measure (SSIM) give the estimations of the different quantitative proportions of the fused images acquired by the MIFT-DWNRT and Existing methodology. The higher estimations of PSNR, Entropy, and SSIM for the fused images demonstrate that the fused images gotten by the MIFT-DWNRT have more data content than the source images. It is observed from the Table I that the standard deviation (SD) estimations of the fused images are higher which shows that the fused images acquired by MIFT-DWNRT technique have higher differentiation than the existing methodology. The most noteworthy estimation of the intertwined image gotten by MIFT-DWNRT technique has more action and clearness level than the source images.

Restorative images of different modalities contain substantial measure of edges and direction highlights, which are regularly exceptionally inconspicuous in nature. MIFT-DWNRT technique attempts to join these correlative and also differentiating highlights from source restorative images into one fused image.

Consequently, it is evident from the outcomes and examinations given over that the fused images gotten by MIFT-DWNRT technique are clearer, instructive and have higher difference which is extremely useful for the clinicians in their conclusion and treatment.

REFERENCES

[1]. Agarwal, J., and Bedi, S.S. (2015), "*Implementation of hybrid image fusion technique for feature enhancement in medical diagnosis*", Springer Open Journal – Human-centric Computing and Information Sciences, Vol. 5, No. 3, pp. 1-17.

[2]. Baum, K.G., Helguera, M., Hornak, J.P., Kerekes, J.P., Montag, E.D., Unlu, M.Z., Feiglin, D.H., and Krol, A. (2006), "*Techniques for Fusion of Multimodal Images: Application to Breast Imaging*", IEEE Transaction on Image Processing, Vol. 9, No. 6, pp. 2521-2524.

[3]. Bhanusree, C., and Chowdary, A.R. (2013), "*A Novel Approach of image fusion MRI and CT image using Wavelet family*", International Journal of Application or Innovation in Engineering & Management, Vol. 2, No. 8, pp. 1-4.

[4]. Da, C., Zhou, A.J., and Do, M. (2006), "*The nonsubsampled contourlet transform: Theory, design, and applications*", IEEE Transactions on Image Processing, Vol. 15, No. 10, pp. 3089 – 3101.

[5]. Das, S., and Kundu, M.K. (2015), "*A Neuro-Fuzzy Approach for Medical Image Fusion*", IEEE Transactions on Biomedical Engineering, Vol. 62, No. 4, pp. 3347-3353.

[6]. Das, S., Chowdhury, M., and Kundu, M.K. (2011), "*Medical image fusion based on ripplet transform type-I*", Progress in Electro-magnetic Research, Vol. 30, No. 3, pp. 355–370.

[7]. Do, M.N., and Vetterli, M. (2005), "*The contourlet transform: an efficient directional multiresolution image representation*", IEEE Transactions on image processing, Vol. 14, No. 12, pp. 2091-2106.

[8]. James, A.P., and Dasarathy, B.V. (2014), "*Medical image fusion: A survey of the state of the art*", Elsevier Information Fusion, Vol. 19, No. 14, pp. 4-19.

[9]. Li, M., Cai, W., and Tan, Z. (2006), "*A region-based multi-sensor image fusion scheme using pulse-coupled neural network*", Pattern Recognition Letters, Vol. 27, No. 16, pp. 1948–1956.

[10]. Mittal, D., and Vaithyanathan, V. (2012), "*An efficient method to improve the spatial property of medical images*", Journal of Theoretical and Applied Information Technology, Vol. 35, No. 2, pp. 141–148.

[11]. Oberoi, A., and Singh, M. (2012), "*Content Based Image Retrieval System for Medical Databases (CBIR-MD) – Lucratively tested on Endoscopy, Dental and Skull Images*", IJCSI International Journal of Computer Science, Vol. 9, No. 1, pp. 300-306.

[12]. Patel, J.M., and Parisk, M.C. (2016), "*Medical Image Fusion Based on Multi-Scaling (DRT) and Multi-Resolution (DWT) Techniques*", IEEE – International Conference on Communication and Signal Processing, Vol. 10, No. 9, pp. 0654-0657.

[13]. Qu, G.H., Zhang, D.L., and Yan, P.F. (2002), "*Information measure for performance of image fusion*", Electronics Letters, Vol. 38, No. 7, pp. 313–315.

[14]. Rajkumar, S., Bardhan, P., Akkireddy, S.K., and Munshi, C. (2014), "*CT and MRI Image Fusion based on Wavelet Transform and Neuro-Fuzzy concepts with quantitative analysis*", IEEE – International Conference on Electronics and Communication Systems, Vol. 8, No. 97, pp. 1-6.

[15]. Wang, Z., and Ma, Y. (2008), "*Medical image fusion using m-PCNN*", Information Fusion, Vol. 9, No. 2, pp. 176–185.

[16]. Wang, Z., Ma, Y., Cheng, F., and Yang, L. (2010), "*Review of pulse-coupled neural networks*", Image Vision Computing, Vol. 28, No. 1, pp. 5–13.

[17]. Wang, Z., Ma, Y., and Gu, J. (2010), "*Multi-focus image fusion using PCNN*", Pattern Recognition, Vol. 43, No. 6, pp. 2003–2016.

[18]. Xu, J., Yang, L., and Wu, D. (2010), "*Ripplet: A new transform for image processing*", Elsevier Journal of Visual Communication & Image Representation, Vol. 21, No. 10, pp. 627-639.

[19]. Xu, Z. (2014), "*Medical image fusion using multi-level local extrema*", Elsevier – Information Fusion, Vol. 19, No. 10, pp. 38-48.

[20]. Yang, L., Guo, B.L., and Ni, W. (2008), "*Multimodality medical image fusion based on multiscale geometric analysis of contourlet transform*", Neurocomputing, Vol. 72, No. 1, pp. 203–211.

[21]. Yang, Y., Park, D.S., Huang, S., and Rao, N. (2010), "*Medical image fusion via an effective wavelet-based approach*", EURASIP Journal on Advances in Signal Processing, Vol. 44, No. 1, pp. 44-53.

[22]. Zhan, L., and Ji, X. (2016), "*CT and MR Images Fusion Method Based on Nonsubsampled Contourlet Transform*", IEEE Transaction - International Conference on Intelligent Human-Machine Systems and Cybernetics, Vol. 10, No. 8, pp. 257-260.